

Nuclear Modification Factors for Hadrons at Forward and Backward Rapidities in Deuteron-Gold Collisions at $\sqrt{s_{NN}} = 200$ GeV

S. S. Adler,⁵ S. Afanasiev,²⁰ C. Aidala,¹⁰ N. N. Ajitanand,⁴⁴ Y. Akiba,^{21,40} A. Al-Jamel,³⁵ J. Alexander,⁴⁴ K. Aoki,²⁵ L. Aphecetche,⁴⁶ R. Armendariz,³⁵ S. H. Aronson,⁵ R. Averbeck,⁴⁵ T. C. Awes,³⁶ V. Babintsev,¹⁷ A. Baldisseri,¹¹ K. N. Barish,⁶ P. D. Barnes,²⁸ B. Bassalleck,³⁴ S. Bathe,^{6,31} S. Batsouli,¹⁰ V. Baublis,³⁹ F. Bauer,⁶ A. Bazilevsky,^{5,41} S. Belikov,^{19,17} M. T. Bjornrdal,¹⁰ J. G. Boissevain,²⁸ H. Borel,¹¹ M. L. Brooks,²⁸ D. S. Brown,³⁵ N. Bruner,³⁴ D. Bucher,³¹ H. Buesching,^{5,31} V. Bumazhnov,¹⁷ G. Bunce,^{5,41} J. M. Burward-Hoy,^{28,27} S. Butsyk,⁴⁵ X. Camard,⁴⁶ P. Chand,⁴ W. C. Chang,² S. Chernichenko,¹⁷ C. Y. Chi,¹⁰ J. Chiba,²¹ M. Chiu,¹⁰ I. J. Choi,⁵³ R. K. Choudhury,⁴ T. Chujo,⁵ V. Ciencialo,³⁶ Y. Cobigo,¹¹ B. A. Cole,¹⁰ M. P. Comets,³⁷ P. Constantin,¹⁹ M. Csanád,¹³ T. Csörgő,²² J. P. Cussonneau,⁴⁶ D. d'Enterria,¹⁰ K. Das,¹⁴ G. David,⁵ F. Deák,¹³ H. Delagrange,⁴⁶ A. Denisov,¹⁷ A. Deshpande,⁴¹ E. J. Desmond,⁵ A. Devismes,⁴⁵ O. Dietzsch,⁴² J. L. Drachenberg,¹ O. Drapier,²⁶ A. Drees,⁴⁵ A. Durum,¹⁷ D. Dutta,⁴ V. Dzhordzhadze,⁴⁷ Y. V. Efremenko,³⁶ H. En'yo,^{40,41} B. Espagnon,³⁷ S. Esumi,⁴⁹ D. E. Fields,^{34,41} C. Finck,⁴⁶ F. Fleuret,²⁶ S. L. Fokin,²⁴ B. D. Fox,⁴¹ Z. Fraenkel,⁵² J. E. Frantz,¹⁰ A. Franz,⁵ A. D. Frawley,¹⁴ Y. Fukao,^{25,40,41} S.-Y. Fung,⁶ S. Gadrat,²⁹ M. Germain,⁴⁶ A. Glenn,⁴⁷ M. Gonin,²⁶ J. Gosset,¹¹ Y. Goto,^{40,41} R. Granier de Cassagnac,²⁶ N. Grau,¹⁹ S. V. Greene,⁵⁰ M. Grosse Perdekamp,^{18,41} H.-Å. Gustafsson,³⁰ T. Hachiya,¹⁶ J. S. Haggerty,⁵ H. Hamagaki,⁸ A. G. Hansen,²⁸ E. P. Hartouni,²⁷ M. Harvey,⁵ K. Hasuko,⁴⁰ R. Hayano,⁸ X. He,¹⁵ M. Heffner,²⁷ T. K. Hemmick,⁴⁵ J. M. Heuser,⁴⁰ P. Hidas,²² H. Hiejima,¹⁸ J. C. Hill,¹⁹ R. Hobbs,³⁴ W. Holzmann,⁴⁴ K. Homma,¹⁶ B. Hong,²³ A. Hoover,³⁵ T. Horaguchi,^{40,41,48} T. Ichihara,^{40,41} V. V. Ikonnikov,²⁴ K. Imai,^{25,40} M. Inaba,⁴⁹ M. Inuzuka,⁸ D. Isenhower,¹ L. Isenhower,¹ M. Ishihara,⁴⁰ M. Issah,⁴⁴ A. Isupov,²⁰ B. V. Jacak,⁴⁵ J. Jia,⁴⁵ O. Jinnouchi,^{40,41} B. M. Johnson,⁵ S. C. Johnson,²⁷ K. S. Joo,³² D. Jouan,³⁷ F. Kajihara,⁸ S. Kametani,^{8,51} N. Kamihara,^{40,48} M. Kaneta,⁴¹ J. H. Kang,⁵³ K. Katou,⁵¹ T. Kawabata,⁸ A. Kazantsev,²⁴ S. Kelly,^{9,10} B. Khachaturov,⁵² A. Khanzadeev,³⁹ J. Kikuchi,⁵¹ D. J. Kim,⁵³ E. Kim,⁴³ G.-B. Kim,²⁶ H. J. Kim,⁵³ E. Kinney,⁹ A. Kiss,¹³ E. Kistenev,⁵ A. Kiyomichi,⁴⁰ C. Klein-Boesing,³¹ H. Kobayashi,⁴¹ L. Kochenda,³⁹ V. Kochetkov,¹⁷ R. Kohara,¹⁶ B. Komkov,³⁹ M. Konno,⁴⁹ D. Kotchetkov,⁶ A. Kozlov,⁵² P. J. Kroon,⁵ C. H. Kuberg,¹ G. J. Kunde,²⁸ K. Kurita,⁴⁰ M. J. Kweon,²³ Y. Kwon,⁵³ G. S. Kyle,³⁵ R. Lacey,⁴⁴ J. G. Lajoie,¹⁹ Y. Le Bornec,³⁷ A. Lebedev,^{19,24} S. Leckey,⁴⁵ D. M. Lee,²⁸ M. J. Leitch,²⁸ M. A. L. Leite,⁴² X. H. Li,⁶ H. Lim,⁴³ A. Litvinenko,²⁰ M. X. Liu,²⁸ C. F. Maguire,⁵⁰ Y. I. Makdisi,⁵ A. Malakhov,²⁰ V. I. Manko,²⁴ Y. Mao,^{38,40} G. Martinez,⁴⁶ H. Masui,⁴⁹ F. Matathias,⁴⁵ T. Matsumoto,^{8,51} M. C. McCain,¹ P. L. McGaughey,²⁸ Y. Miake,⁴⁹ T. E. Miller,⁵⁰ A. Milov,⁴⁵ S. Mioduszewski,⁵ G. C. Mishra,¹⁵ J. T. Mitchell,⁵ A. K. Mohanty,⁴ D. P. Morrison,⁵ J. M. Moss,²⁸ D. Mukhopadhyay,⁵² M. Muniruzzaman,⁶ S. Nagamiya,²¹ J. L. Nagle,^{9,10} T. Nakamura,¹⁶ J. Newby,⁴⁷ A. S. Nyanin,²⁴ J. Nystrand,³⁰ E. O'Brien,⁵ C. A. Ogilvie,¹⁹ H. Ohnishi,⁴⁰ I. D. Ojha,^{3,50} H. Okada,^{25,40} K. Okada,^{40,41} A. Oskarsson,³⁰ I. Otterlund,³⁰ K. Oyama,⁸ K. Ozawa,⁸ D. Pal,⁵² A. P. T. Palounek,²⁸ V. Pantuev,⁴⁵ V. Papavassiliou,³⁵ J. Park,⁴³ W. J. Park,²³ S. F. Pate,³⁵ H. Pei,¹⁹ V. Penev,²⁰ J.-C. Peng,¹⁸ H. Pereira,¹¹ V. Peresedov,²⁰ A. Pierson,³⁴ C. Pinkenburg,⁵ R. P. Pisani,⁵ M. L. Purschke,⁵ A. K. Purwar,⁴⁵ J. M. Qualls,¹ J. Rak,¹⁹ I. Ravinovich,⁵² K. F. Read,^{36,47} M. Reuter,⁴⁵ K. Reygers,³¹ V. Riabov,³⁹ Y. Riabov,³⁹ G. Roche,²⁹ A. Romana,²⁶ M. Rosati,¹⁹ S. S. E. Rosendahl,³⁰ P. Rosnet,²⁹ V. L. Rykov,⁴⁰ S. S. Ryu,⁵³ N. Saito,^{25,40,41} T. Sakaguchi,^{8,51} S. Sakai,⁴⁹ V. Samsonov,³⁹ L. Sanfratello,³⁴ R. Santo,³¹ H. D. Sato,^{25,40} S. Sato,^{5,49} S. Sawada,²¹ Y. Schutz,⁴⁶ V. Semenov,¹⁷ R. Seto,⁶ T. K. Shea,⁵ I. Shein,¹⁷ T.-A. Shibata,^{40,48} K. Shigaki,¹⁶ M. Shimomura,⁴⁹ A. Sickles,⁴⁵ C. L. Silva,⁴² D. Silvermyr,²⁸ K. S. Sim,²³ A. Soldatov,¹⁷ R. A. Soltz,²⁷ W. E. Sondheim,²⁸ S. P. Sorensen,⁴⁷ I. V. Sourikova,⁵ F. Staley,¹¹ P. W. Stankus,³⁶ E. Stenlund,³⁰ M. Stepanov,³⁵ A. Ster,²² S. P. Stoll,⁵ T. Sugitate,¹⁶ J. P. Sullivan,²⁸ S. Takagi,⁴⁹ E. M. Takagui,⁴² A. Taketani,^{40,41} K. H. Tanaka,²¹ Y. Tanaka,³³ K. Tanida,⁴⁰ M. J. Tannenbaum,⁵ A. Taranenko,⁴⁴ P. Tarján,¹² T. L. Thomas,³⁴ M. Togawa,^{25,40} J. Tojo,⁴⁰ H. Torii,^{25,41} R. S. Towell,¹ V.-N. Tram,²⁶ I. Tserruya,⁵² Y. Tsuchimoto,¹⁶ H. Tydesjö,³⁰ N. Tyurin,¹⁷ T. J. Uam,³² H. W. van Hecke,²⁸ J. Velkovska,⁵ M. Velkovsky,⁴⁵ V. Veszprémi,¹² A. A. Vinogradov,²⁴ M. A. Volkov,²⁴ E. Vznuzdaev,³⁹ X. R. Wang,¹⁵ Y. Watanabe,^{40,41} S. N. White,⁵ N. Willis,³⁷ F. K. Wohn,¹⁹ C. L. Woody,⁵ W. Xie,⁶ A. Yanovich,¹⁷ S. Yokkaichi,^{40,41} G. R. Young,³⁶ I. E. Yushmanov,²⁴ W. A. Zajc,^{10,*} C. Zhang,¹⁰ S. Zhou,⁷ J. Zimányi,²² L. Zolin,²⁰ and X. Zong¹⁹

(PHENIX Collaboration)

¹Abilene Christian University, Abilene, Texas 79699, USA

²Institute of Physics, Academia Sinica, Taipei 11529, Taiwan

³Department of Physics, Banaras Hindu University, Varanasi 221005, India

- ⁴Bhabha Atomic Research Centre, Bombay 400 085, India
⁵Brookhaven National Laboratory, Upton, New York 11973-5000, USA
⁶University of California–Riverside, Riverside, California 92521, USA
⁷China Institute of Atomic Energy (CIAE), Beijing, People’s Republic of China
⁸Center for Nuclear Study, Graduate School of Science, University of Tokyo, 7-3-1 Hongo, Bunkyo, Tokyo 113-0033, Japan
⁹University of Colorado, Boulder, Colorado 80309, USA
¹⁰Columbia University, New York, New York 10027, USA and Nevis Laboratories, Irvington, New York 10533, USA
¹¹Dapnia, CEA Saclay, F-91191, Gif-sur-Yvette, France
¹²Debrecen University, H-4010 Debrecen, Egyetem tér 1, Hungary
¹³ELTE, Eötvös Loránd University, H-1117 Budapest, Pázmány P. s. 1/A, Hungary
¹⁴Florida State University, Tallahassee, Florida 32306, USA
¹⁵Georgia State University, Atlanta, Georgia 30303, USA
¹⁶Hiroshima University, Kagamiyama, Higashi-Hiroshima 739-8526, Japan
¹⁷Institute for High Energy Physics (IHEP), Protvino, Russia
¹⁸University of Illinois at Urbana-Champaign, Urbana, Illinois 61801, USA
¹⁹Iowa State University, Ames, Iowa 50011, USA
²⁰Joint Institute for Nuclear Research, 141980 Dubna, Moscow Region, Russia
²¹KEK, High Energy Accelerator Research Organization, Tsukuba-shi, Ibaraki-ken 305-0801, Japan
²²KFKI Research Institute for Particle and Nuclear Physics (RMKI), H-1525 Budapest 114, PO Box 49, Hungary
²³Korea University, Seoul, 136-701, Korea
²⁴Russian Research Center “Kurchatov Institute,” Moscow, Russia
²⁵Kyoto University, Kyoto 606, Japan
²⁶Laboratoire Leprince-Ringuet, Ecole Polytechnique, CNRS-IN2P3, Route de Saclay, F-91128, Palaiseau, France
²⁷Lawrence Livermore National Laboratory, Livermore, California 94550, USA
²⁸Los Alamos National Laboratory, Los Alamos, New Mexico 87545, USA
²⁹LPC, Université Blaise Pascal, CNRS-IN2P3, Clermont-Fd, 63177 Aubiere Cedex, France
³⁰Department of Physics, Lund University, Box 118, SE-221 00 Lund, Sweden
³¹Institut für Kernphysik, University of Muenster, D-48149 Muenster, Germany
³²Myongji University, Yongin, Kyonggido 449-728, Korea
³³Nagasaki Institute of Applied Science, Nagasaki-shi, Nagasaki 851-0193, Japan
³⁴University of New Mexico, Albuquerque, New Mexico 87131, USA
³⁵New Mexico State University, Las Cruces, New Mexico 88003, USA
³⁶Oak Ridge National Laboratory, Oak Ridge, Tennessee 37831, USA
³⁷IPN-Orsay, Université Paris Sud, CNRS-IN2P3, BP1, F-91406, Orsay, France
³⁸Peking University, Beijing, People’s Republic of China
³⁹PNPI, Petersburg Nuclear Physics Institute, Gatchina, Russia
⁴⁰RIKEN (The Institute of Physical and Chemical Research), Wako, Saitama 351-0198, Japan
⁴¹RIKEN BNL Research Center, Brookhaven National Laboratory, Upton, New York 11973-5000, USA
⁴²Universidade de São Paulo, Instituto de Física, Caixa Postal 66318, São Paulo CEP05315-970, Brazil
⁴³System Electronics Laboratory, Seoul National University, Seoul, South Korea
⁴⁴Chemistry Department, Stony Brook University, SUNY, Stony Brook, New York 11794-3400, USA
⁴⁵Department of Physics and Astronomy, Stony Brook University, SUNY, Stony Brook, New York 11794, USA
⁴⁶SUBATECH (Ecole des Mines de Nantes, CNRS-IN2P3, Université de Nantes), BP 20722-44307, Nantes, France
⁴⁷University of Tennessee, Knoxville, Tennessee 37996, USA
⁴⁸Department of Physics, Tokyo Institute of Technology, Tokyo, 152-8551, Japan
⁴⁹Institute of Physics, University of Tsukuba, Tsukuba, Ibaraki 305, Japan
⁵⁰Vanderbilt University, Nashville, Tennessee 37235, USA
⁵¹Waseda University, Advanced Research Institute for Science and Engineering, 17 Kikui-cho, Shinjuku-ku, Tokyo 162-0044, Japan
⁵²Weizmann Institute, Rehovot 76100, Israel
⁵³Yonsei University, IPAP, Seoul 120-749, Korea

(Received 29 November 2004; published 3 March 2005)

We report on charged hadron production in deuteron-gold reactions at $\sqrt{s_{NN}} = 200$ GeV. Our measurements in the deuteron direction cover $1.4 < \eta < 2.2$, referred to as forward rapidity, and in the gold direction $-2.0 < \eta < -1.4$, referred to as backward rapidity, and a transverse momentum range $p_T = 0.5\text{--}4.0$ GeV/c. We compare the relative yields for different deuteron-gold collision centrality classes. We observe a suppression relative to binary collision scaling at forward rapidity, sensitive to low momentum fraction (x) partons in the gold nucleus, and an enhancement at backward rapidity, sensitive to high momentum fraction partons in the gold nucleus.

Deep inelastic scattering of leptons on the proton revealed the proton's substructure of pointlike parton constituents [1]. This substructure, usually described quantitatively as parton distribution functions, evolves as one probes the proton at shorter wavelength or equivalently higher momentum transfer, Q^2 . Using the measured quark and antiquark distribution functions and the DGLAP [2] and BFKL [3] evolution equations, a strong increase in the gluon density is expected at high Q^2 and small x (fraction of the proton momentum carried by the parton). Such an increase is, indeed, observed at HERA [4], suggesting that at sufficiently small x , gluons should overlap in space and time. This overlap should result in gluon fusion, and thus reduce the gluon density at low x and enhance it at larger x . This gluon fusion limits the achievable gluon density, leading to gluon saturation. This saturation is sometimes described as the formation of a color glass condensate [5]. Gluon saturation is expected to be a larger effect in nuclei where the partons from different nucleons overlap as well. Suppression of low x partons in nuclei relative to nucleons has been experimentally observed and is referred to as nuclear shadowing [6]. However, this shadowing is often described in terms of modification of the leading-twist parton densities in nuclei [7].

In 2003 the Relativistic Heavy Ion Collider (RHIC) collided deuteron and gold nuclei at $\sqrt{s_{NN}} = 200$ GeV. At this energy, most hadrons with $p_T > 2.0$ GeV/ c arise from parton-parton interactions and can be used as a probe of nuclear partonic structure. Hadrons with $p_T > 2.0$ GeV/ c at forward rapidity $1.4 < \eta < 2.2$ are sensitive to low x partons in the gold nucleus $0.001 < x < 0.03$. Hadrons at backward rapidity $-2.0 < \eta < -1.4$ are sensitive to high x partons in the gold nucleus $0.04 < x < 0.5$. It has been predicted that gluon saturation at small x will suppress hadronic yields at forward rapidity [8] with the transverse momentum scale for the onset of the gluon saturation set by $Q_s^2[\text{GeV}^2] = 0.13 N_{\text{coll}} e^{\lambda y}$ [9] for $d + \text{Au}$ collisions at RHIC. Here $\lambda \sim 0.3$ is determined from HERA data [10] and N_{coll} is the number of nucleon-nucleon inelastic collisions. Thus, for central collisions and within our forward rapidity coverage Q_s^2 is expected to be of order 2–4 GeV² and may have observable consequences. Novel hadron production mechanisms, such as quark recombination [11], can also impact the distribution of particles in the forward rapidity region.

Results on charged hadron yields at forward rapidity from the BRAHMS experiment have shown a suppression of the yield of hadrons in central, compared to peripheral, $d + \text{Au}$ collisions [12]. At midrapidity, PHENIX has reported a modest enhancement of the yield of hadrons with $p_T > 1.5$ GeV/ c [13]. This enhancement, generally referred to as the “Cronin effect” is often ascribed to initial state scattering of the parton traversing the nucleus prior to the high Q^2 scattering [14]. At backward rapidities (large x), antishadowing and other effects of the surrounding

nuclear medium (e.g., the EMC effect) [15] may compete, making predictions challenging.

It is important to note that in the transverse momentum range of this measurement, $0.5 < p_T < 4.0$ GeV/ c , hadron production is also sensitive to soft physics phenomena which are determined by coherent hadron-hadron interactions. In $p + A$ reactions at lower energies soft hadron production shifts from forward to backward rapidity, with a larger shift for larger nuclear targets. Thus, at low p_T one may observe an increase (decrease) in hadron yields at backward (forward) rapidity which is not necessarily a reflection of changes at the partonic structure level.

In this Letter, we present results from the PHENIX experiment [16] on the ratio of hadron yields at forward and backward pseudorapidity for different centrality classes of $d + \text{Au}$ collisions. PHENIX has two spectrometers designed for measuring muon production over the pseudorapidity range $-2.2 < \eta < -1.2$ (backward spectrometer) and $1.2 < \eta < 2.4$ (forward spectrometer) [16]. The spectrometers start with a thick hadron absorber composed of 19 cm of brass and 60 cm of low-carbon steel between the collision point and active detectors along the beam axis, primarily to reduce hadronic background for muon measurements [17]. After this material, the Muon Tracker (MuTr) detector, consisting of three stations of cathode strip chambers, tracks charged particles in a magnetic field. The momentum resolution is 5% (for typical momenta in this analysis) and the absolute scale is known to better than 1%. Following the muon magnet backplate [30 (20) cm of steel in the forward (backward) spectrometer] there is a Muon Identifier (MuID) detector. The MuID consists of five layers of planar drift tubes interleaved with layers of steel for further hadron absorption (10 cm thick in the first two layers and 20 cm thick for the remaining layers). The layers are numbered 0–4, with 4 being the most downstream. The MuID is used to separate muons from hadrons and provide triggering capabilities.

Although these spectrometers were designed to detect muons, they can also be used to measure charged hadrons via two independent methods. The first method is via the identification of hadrons which penetrate part way through the MuID, referred to as “punch-through hadrons.” The second method is via muons from light mesons π , K which decay before interacting in the absorber material. By measuring these decay muons, we can reconstruct the yield of their parent light mesons. In both of these methods the absolute yield of hadrons is difficult to determine due to uncertainties in the punch-through and decay probabilities. However, this small probability is independent of $d + \text{Au}$ collision centrality, and thus not knowing the absolute yields does not affect the precision of measured ratios of hadron yields between the different classes of events.

The punch-through hadron identification is achieved by studying particles that stop somewhere within the MuID before the last layer. For muons penetrating up to layers 2

and 3 we expect the average momenta measured in the MuTr of $p = 1.0$ and 1.2 GeV/ c , respectively, corresponding to the average ionization energy loss in traversing the spectrometer material. The reconstructed momentum distributions for particles stopping in layers 2 and 3 of the MuID are shown in Fig. 1. In addition to the expected muon peaks, there is a broad distribution extending to higher momentum which is the result of punch-through hadrons. These hadrons also suffer ionization energy loss up to the relevant layer, then suffer an inelastic collision in the MuID steel, and do not penetrate further. We thus select a clean sample of hadrons by demanding that a track stop in MuID layer 2 or 3 and have momentum more than 3σ away from the muon peaks. Muon contamination in our sample is estimated from simulations to be less than 5%.

Another source of background for the punch-through hadrons is secondary particles produced from hadronic showering in the absorber. This background is reduced by requiring that the track point back to the primary collision vertex, as determined from the beam-beam counter (BBC). The background from secondary particles varies as a function of p_T and is typically $\sim 1\%$ – 5% of the signal based on simulations. We also apply acceptance cuts $-2.0 < \eta < -1.4$ and $1.4 < \eta < 2.2$ in order to reduce the background at small angles.

Some hadrons will decay into muons before the absorber, and the decay muons are then measured by the muon spectrometers. Muons can result from many sources including decays of π , K , D mesons, and J/ψ . These particles have a finite decay probability P_{decay} before they reach the absorber

$$P_{\text{decay}}(p, L) = 1 - e^{-Lm/\tau p}, \quad (1)$$

where $L \sim 41$ cm is the distance from the collision vertex to the absorber; p , m , and τ are the momentum, mass, and proper lifetime of the parent particle.

Thus, collisions that occur far from the absorber are more likely to produce muons from light meson decays than those that occur close to the absorber. Charm hadrons,

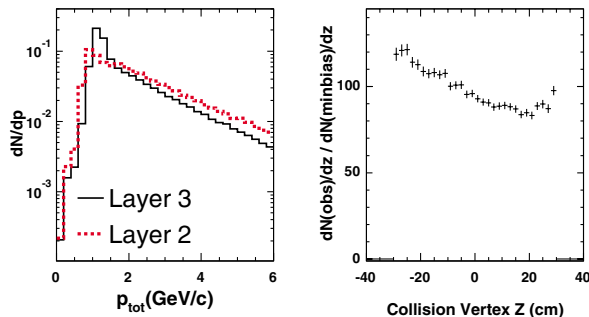


FIG. 1 (color online). Left: The total momentum p_{tot} measured in the MuTr without energy loss correction of all charged tracks penetrating to MuID layers 2 (gray) and 3 (black). Right: Collision vertex distribution for events with muons at forward rapidity, corrected for the minimum bias collision vertex distribution.

however, due to their very short proper decay lengths, $e^{-Lm/\tau p} \ll 1$, will have minimal collision vertex dependence. The right panel of Fig. 1 shows the collision vertex distribution from events in which muons are detected at forward rapidity, corrected for the minimum bias collision vertex distribution. The large vertex dependence indicates a significant fraction of the muons are from pion and kaon decay. Using this distribution, we can separate the muons from pion and kaon decay from other contributions. The acceptance and efficiency vary by less than 5% over the z vertex range, which establishes an upper bound on the systematic error attributable to the subtraction of these nonsignal contributions. It should be noted that the measured muon p_T is approximately 15% lower on average than the parent hadron p_T , which is not corrected for in this analysis.

The data set for this analysis was collected under two different trigger conditions. We recorded 67×10^6 minimum bias triggers which required at least one hit in both the PHENIX forward $3.0 < \eta < 3.9$ and backward $-3.9 < \eta < -3.0$ BBC and a reconstructed vertex position within $|z| < 30$ cm along the beam axis. The minimum bias trigger accepts $88\% \pm 4\%$ of all inelastic $d + \text{Au}$ collisions [13]. The second data set, sampling 5.3×10^9 minimum bias events, was collected with the MuID trigger which requires at least one track penetrating the first four layers of the MuID.

We divide these events into four centrality classes based on the number of particle hits in the backward BBC counter covering $-3.9 < \eta < -3.0$. Using a Glauber model [13] and simulation of the BBC, we determine the average number of binary collisions in each centrality class. The classes are categorized as follows: 60%–88% ($\langle N_{\text{coll}} \rangle = 3.1 \pm 0.3$), 40%–60% ($\langle N_{\text{coll}} \rangle = 7.0 \pm 0.6$), 20%–40% ($\langle N_{\text{coll}} \rangle = 10.6 \pm 0.7$), and 0%–20% ($\langle N_{\text{coll}} \rangle = 15.4 \pm 1.0$).

There is a correlation between having a particular physics process (for example, the production of a high p_T hadron) and the BBC response. The BBC coverage in pseudorapidity is well separated from the muon spectrometers so the correlation is not predominantly due to jet fragmentation, but rather an underlying event correlation. We have studied this effect in detail using proton-proton and $d + \text{Au}$ data, as well as in simulations, and have accounted for this correlation bias. The bias correction factors we apply range from 0%–7% depending on the centrality category and the physics process. The systematic errors on these corrections are less than 4%.

The nuclear modification factor R_{cp} is defined as the ratio of the particle yield in central collisions to the particle yield in peripheral collisions, each normalized by the average number of nucleon-nucleon binary collisions ($\langle N_{\text{coll}} \rangle$):

$$R_{cp} = \frac{\langle \left(\frac{dN}{d\eta dp_T} \right)_{\text{central}} \rangle / \langle N_{\text{coll}}^{\text{central}} \rangle}{\langle \left(\frac{dN}{d\eta dp_T} \right)_{\text{peripheral}} \rangle / \langle N_{\text{coll}}^{\text{peripheral}} \rangle}. \quad (2)$$

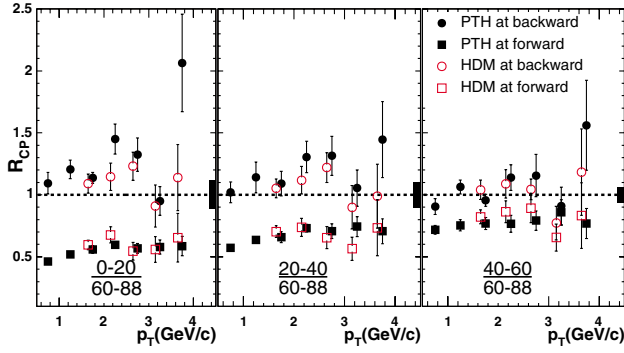


FIG. 2 (color online). R_{CP} as a function of p_T at forward rapidity (squares) and backward rapidity (circles) for different centrality classes.

The hadron R_{CP} , using the most peripheral centrality class (60%–88%) for normalization, is shown in Fig. 2 as a function of p_T at forward and backward rapidities. The results from the punch-through hadron and hadron decay muon techniques are both shown and are in quite good agreement. We also show the results integrated over $1.5 < p_T < 4.0$ GeV/c as a function of pseudorapidity in Fig. 3.

There are two types of systematic uncertainties in our analysis. Common systematic errors which move all data points up and down together include the error on $\frac{N_{coll}^{central}}{N_{coll}^{peripheral}}$ (10.8% for the most central bin), the centrality bias correction factors (4%), and the centrality-dependent tracking efficiency (4%) determined by embedding Monte Carlo particles in real data. Common systematic errors are shown as a black bar. Point-to-point systematic errors result from sensitivities to analysis cuts and are 5%–10%. They are added in quadrature with the statistical errors and shown as error bars.

It is notable that our two measurement methods have different sensitivity to different hadrons. The particle composition ($\pi/K/p$ ratio) of the observed sample is modified relative to the particle composition at the collision vertex due to species-dependent nuclear interaction cross sections affecting the punch-through hadrons and due to species-

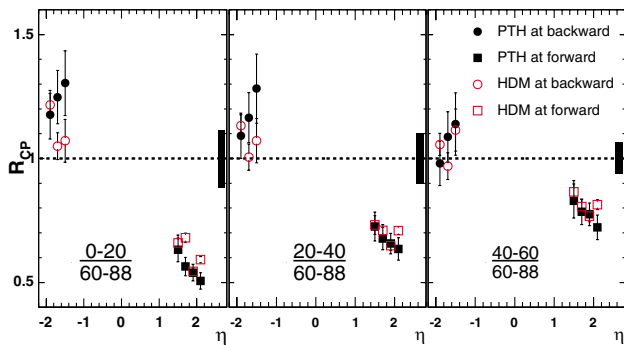


FIG. 3 (color online). R_{CP} as a function of η for $1.5 < p_T < 4.0$ GeV/c for different centrality classes.

dependent decay lifetimes affecting the hadron decay muons. Both effects enhance the kaon contribution to our R_{CP} measurements. The uncertainty on our charged hadron R_{CP} values introduced by this effect is estimated to be less than 4% by calculating the difference between the kaon R_{CP} and inclusive charged particle R_{CP} determined by PHENIX at midrapidity [18].

We observe that R_{CP} shows a suppression at forward rapidity that is largest for the most central events. The opposite trend is observed at backward rapidity where R_{CP} shows an enhancement that is also largest for the most central events. We observe a weak p_T dependence with slightly smaller R_{CP} values at lower p_T . We observe a clear pseudorapidity dependence at forward rapidity with R_{CP} dropping further at larger η values. Within our current uncertainties we are unable to discern any pseudorapidity dependence at backward rapidity.

In Fig. 4 we compare results from the BRAHMS experiment [12] with our results at forward rapidity. The PHENIX data and the BRAHMS data are in agreement within systematic uncertainties.

The suppression of hadron yields relative to binary collision scaling at forward rapidity is expected from initial state nuclear effects. However, detailed comparisons with various theoretical approaches is necessary in order to discriminate between different models. In particular, the lack of a strong p_T dependence at both forward and backward rapidities must be understood as the physics processes transition from “soft” to “hard” physics scales.

To summarize, we observe a suppression in hadron yields relative to binary collision scaling at forward rapidities and an enhancement at backward rapidity for central relative to peripheral $d + Au$ reactions at $\sqrt{s_{NN}} = 200$ GeV. The forward rapidity suppression is in qualitative agreement with the expectation of shadowing and saturation effects in the small x region in the gold nucleus.

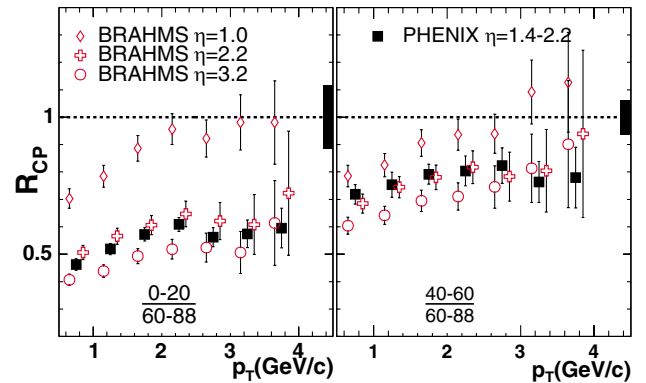


FIG. 4 (color online). PHENIX R_{CP} as a function of p_T at forward rapidities shown as the average of the two methods. Note that the BRAHMS results are for negative hadrons at $\eta = 2.2$ and 3.2 , and their centrality ranges (0%–20%/60%–80% and 30%–50%/60%–80%) are somewhat different from ours.

However, other physics effects must also be considered in understanding the full p_T and η dependence. The source of the backward rapidity enhancement, and the possible contribution of antishadowing of large x partons, has yet to be understood.

We thank the staff of the Collider-Accelerator and Physics Departments at BNL for their vital contributions. We acknowledge support from the Department of Energy and NSF (U.S.A.), MEXT and JSPS (Japan), CNPq and FAPESP (Brazil), NSFC (China), IN2P3/CNRS, CEA, and ARMINES (France), BMBF, DAAD, and AvH (Germany), OTKA (Hungary), DAE and DST (India), ISF (Israel), KRF and CHEP (Korea), RMIST, RAS, and RMAE (Russia), VR and KAW (Sweden), U.S. CRDF for the FSU, U.S.-Hungarian NSF-OTKA-MTA, and U.S.-Israel BSF.

*PHENIX Spokesperson.

Electronic address: zajc@nevis.columbia.edu

- [1] J.D. Bjorken and E.A. Paschos, Phys. Rev. **185**, 1975 (1969).
- [2] G. Altarelli and G. Parisi, Nucl. Phys. **B126**, 298 (1977); Y.L. Dokshitzer, Sov. Phys. JETP **46**, 641 (1977); V.N. Gribov and L.N. Lipatov, Sov. J. Nucl. Phys. **15**, 438 (1972).
- [3] I. I. Balitsky and L. N. Lipatov, Sov. J. Nucl. Phys. **28**, 822 (1978); E. A. Kuraev, L. N. Lipatov, and V. S. Fadin, Sov. Phys. JETP **45**, 199 (1977); **44**, 443 (1976).
- [4] H. Abramowicz and A. C. Caldwell, Rev. Mod. Phys. **71**, 1275 (1999).
- [5] L. McLerran and R. Venugopalan, Phys. Rev. D **49**, 2233 (1994); **49**, 3352 (1994).
- [6] J. Ashman *et al.*, Phys. Lett. B **202**, 603 (1988).
- [7] V. Guzey, M. Strikman, and W. Vogelsang, hep-ph/0407201.
- [8] A. Dumitru and J. Jalilian-Marian, Phys. Lett. B **547**, 15 (2002); F. Gelis and J. Jalilian-Marian, Phys. Rev. D **66**, 014021 (2002).
- [9] D. Kharzeev, Y. V. Kovchegov, and K. Tuchin, Phys. Lett. B **599**, 23 (2004).
- [10] K. Golec-Biernat and M. Wusthoff, Phys. Rev. D **59**, 014017 (1999); **60**, 114023 (1999).
- [11] R. Hwa, C. B. Yang, and R. J. Fries, nucl-th/0410111.
- [12] I. Arsene *et al.*, Phys. Rev. Lett. **93**, 242303 (2004).
- [13] S. S. Adler *et al.*, Phys. Rev. Lett. **91**, 072303 (2003).
- [14] D. Antreasyan *et al.*, Phys. Rev. D **19**, 764 (1979).
- [15] M. Arneodo, Phys. Rep. **240**, 301 (1994).
- [16] K. Adcox *et al.*, Nucl. Instrum. Methods Phys. Res., Sect. A **499**, 469 (2003), and references therein.
- [17] S. H. Aronson *et al.*, Nucl. Instrum. Methods Phys. Res., Sect. A **499**, 480 (2003).
- [18] F. Matathias *et al.*, J. Phys. G **30**, S1113 (2004).